Materials Today Bio 26 (2024) 101051

Contents lists available at ScienceDirect

Materials Today Bio

journal homepage: www.journals.elsevier.com/materials-today-bio

Trilayered biomimetic hydrogel scaffolds with dual-differential microenvironment for articular osteochondral defect repair

Hongying Chen [a,b,c,1], Jinyi Huang [c,1], Xiaomeng Li [f,1], Weiwei Zhao [a], Yujie Hua [c,d,e,**], Zhenfeng Song [a], Xianwei Wang [b], Zhikun Guo [b], Guangdong Zhou [c,d,e,*], Wenjie Ren [a,b,e,***], Yongkun Sun [a,b,****]

[a] School of Basic Medical Sciences of Xinxiang Medical University, The Third Affiliated Hospital of Xinxiang Medical University, Henan Key Laboratory of Medical and Protective Products, Xinxiang, Henan, 453003, China
[b] The Key Laboratory of Medical Tissue Regeneration in Henan Province of Xinxiang Medical University, Xinxiang, Henan, 453003, China
[c] Department of Plastic and Reconstructive Surgery, Shanghai Ninth People's Hospital Affiliated to Shanghai Jiao Tong University School of Medicine, Shanghai Key Laboratory of Tissue Engineering, Shanghai Jiao Tong University, Shanghai, 200011, China
[d] National Tissue Engineering Center of China, Shanghai, 200241, China
[e] Institute of Regenerative Medicine and Orthopedics, Institutes of Health Central Plain, Xinxiang Medical University, Xinxiang, Henan, 453003, China
[f] School of Mechanics and Safety Engineering, Zhengzhou University, Zhengzhou, Henan, 450001, China

ARTICLE INFO

Keywords:
Osteochondral repair
Trilayered scaffolds
Hydrogels
Microenvironment

ABSTRACT

Commonly, articular osteochondral tissue exists significant differences in physiological architecture, mechanical function, and biological microenvironment. However, the development of biomimetic scaffolds incorporating upper cartilage, middle tidemark-like, and lower subchondral bone layers for precise articular osteochondral repair remains elusive. This study proposed here a novel strategy to construct the trilayered biomimetic hydrogel scaffolds with dual-differential microenvironment of both mechanical and biological factors. The cartilage-specific microenvironment was achieved through the grafting of kartogenin (KGN) into gelatin *via* *p*-hydroxyphenylpropionic acid (HPA)-based enzyme crosslinking reaction as the upper cartilage layer. The bone-specific microenvironment was achieved through the grafting of atorvastatin (AT) into gelatin *via* dual-crosslinked network of both HP-based enzyme crosslinking and glycidyl methacrylate (GMA)-based photo-crosslinking reactions as the lower subchondral bone layer. The introduction of tidemark-like middle layer is conducive to the formation of well-defined cartilage-bone integrated architecture. The *in vitro* experiments demonstrated the significant mechanical difference of three layers, successful grafting of drugs, good cytocompatibility and tissue-specific induced function. The results of *in vivo* experiments also confirmed the mechanical difference of the trilayered bionic scaffold and the ability of inducing osteogenesis and chondrogenesis. Furthermore, the articular osteochondral defects were successfully repaired using the trilayered biomimetic hydrogel scaffolds by the activation of endogenous recovery, which offers a promising alternative for future clinical treatment.

* Corresponding authors. Department of Plastic and Reconstructive Surgery, Shanghai Ninth People's Hospital Affiliated to Shanghai Jiao Tong University School of Medicine, Shanghai Key Laboratory of Tissue Engineering, Shanghai Jiao Tong University, Shanghai, 200011, China.
** Corresponding author. Department of Plastic and Reconstructive Surgery, Shanghai Ninth People's Hospital Affiliated to Shanghai Jiao Tong University School of Medicine, Shanghai Key Laboratory of Tissue Engineering, Shanghai Jiao Tong University, Shanghai, 200011, China.
*** Corresponding author. School of Basic Medical Sciences of Xinxiang Medical University, The Third Affiliated Hospital of Xinxiang Medical University, Henan Key Laboratory of Medical and Protective Products, Xinxiang, Henan, 453003, China.
**** Corresponding author. School of Basic Medical Sciences of Xinxiang Medical University, The Third Affiliated Hospital of Xinxiang Medical University, Henan Key Laboratory of Medical and Protective Products, Xinxiang, Henan, 453003, China.
E-mail addresses: yujiehua@shsmu.edu.cn (Y. Hua), guangdongzhou@126.com (G. Zhou), wjren1966@163.com (W. Ren), sun@xxum.edu.cn (Y. Sun).
[1] These authors contributed equally to this work.

https://doi.org/10.1016/j.mtbio.2024.101051
Received 16 January 2024; Received in revised form 22 March 2024; Accepted 9 April 2024
Available online 10 April 2024

1. Introduction

Articular cartilage is a crucial tissue involved in joint function, serving to bear mechanical loads and reduce friction [1–3]. Injuries to the articular cartilage, resulting from trauma, aging, and degeneration, often extend to the calcified cartilage and subchondral bone layers, leading to the formation of osteochondral defects (OCDs) [4,5]. The severe issue of OCDs gradually evolves from initial joint pain and movement disorder to osteoarthritis, and thus leads to physiologically functional disability. Commonly, articular osteochondral tissue exists significant differences in physiological architecture, mechanical function, and biological microenvironment between cartilage and subchondral bone layers [6,7]. The upper cartilage layer, mainly composed of type II collagen and proteoglycan, presents soft and lubricous tissue surface, which is avascular, aneural, and lacks lymphatic vessels [8,9]. Whereas, the lower subchondral bone layer, full of abundant blood vessels and nerves, has a calcified texture of hardness that exerts the essential function in resistance to mechanical loads [10,11]. Among them, the middle layer of tidemark is to effectively prevent blood vessel and nerve invasions from the subchondral bone into the cartilage tissue, which is important to maintain the dynamic balance of physiological calcification [12].

Currently, conventional treatments for OCDs disease in clinic include microfracture, autograft/allograft transplantation, and total articular replacement [13–15]. However, the therapeutic effect of these treatments is still dissatisfactory due to the lack of ideal transplant donors. Tissue engineering technology has emerged as a promising alternative for OCDs repair. It combines seed cells, biocompatible scaffolds, growth factors, physical stimulation and other factors, to construct living cartilage or bone autografts [16,17]. However, the following problems still need to be resolved: 1) Most previous studies normally used bilayered biomimetic scaffolds to repair both cartilage and subchondral bone [18], but ignored the precise mimicking of tidemark or calcified cartilage zone. Meanwhile, the gradient architecture is simply assembled and the interfacial connection between adjacent layers is prone to separate from each other [19]. 2) Different layers of articular osteochondral tissue have different mechanical functions: the cartilage layer is relatively soft and wet to lubricate the joint cavity; the bone layer is extremely hard to provide mechanical support [20]; the tidemark firmly integrates well with both soft and stiff tissues to maintain the interfacial stability. 3) The biological microenvironment of multilayered biomimetic scaffolds significantly affects the chondrogenic and osteogenic differentiation of stem cells, and thus determines the therapeutic effect of OCDs [21].

Hydrogels are versatile biomaterials that are commonly used in tissue engineering and regenerative medicine. They possess physicochemical properties that closely resemble the natural extracellular matrix, including excellent biocompatibility, biodegradability, favorable mechanical properties, a porous structure, and ease of operation [22].As known, gelatin, a widely employed biomacromolecule, is derived from the partial hydrolysis of collagen. It not only promotes cell adhesion but also enhances tissue regeneration [23]. In the previous studies, gelatin could be crosslinked into three-dimensional network by means of physical and chemical crosslinking approaches. The conventional physical crosslinking or biological crosslinking methods, including pH-response, enzyme crosslinking, and supramolecular assembly, are mechanically weak [24–26]. However, the mechanical strength of ordinary chemical crosslinking methods is relatively high based on the reliable crosslinking bonds, such as multitype of coupling reaction and photo-crosslinking techniques [27,28]. In addition, the introduction of growth factors (*e.g.*, FGF, TGFβ, and BMP-2) is prone to protein denaturation that is hard for long-term preservation, while the small molecular drugs are easy to be grafted into the biomacromolecule for both drugs carrying and releasing [29]. For example, kartogenin (KGN) is considered as an efficient chondrogenic drug [30], while atorvastatin (AT) has a synergetic effect on the promotion of cartilage and bone regeneration [31]. Therefore, how to develop the trilayered biomimetic scaffolds with dual-differential microenvironment of both mechanical and biological factors that suitable for stem cell differentiation and activating endogenous repair remains challenging to realize.

Herein, we proposed a novel strategy to construct the trilayered biomimetic hydrogel scaffolds with dual-differential microenvironment for articular osteochondral defect repair (Fig. 1). The cartilage-specific microenvironment was achieved through the grafting of KGN into gelatin *via p*-hydroxyphenylpropionic acid (HPA)-based enzyme crosslinking reaction as the upper cartilage layer. The bone-specific microenvironment was achieved through the grafting of AT into gelatin *via* dual-crosslinked network of both HP-based enzyme crosslinking and glycidyl methacrylate (GMA)-based photo-crosslinking reactions as the lower subchondral bone layer. The introduction of tidemark-like middle layer is conducive to the formation of well-defined cartilage-bone integrated architecture. Furthermore, *in vitro* experiments demonstrated the significant mechanical difference of three layers, successful grafting of drugs, good cytocompatibility and tissue-specific induced function. Meanwhile, *in vivo* experiments certified the feasibility of repairing articular osteochondral defects using the trilayered biomimetic hydrogel scaffolds by the activation of endogenous recovery, which offers a promising alternative for future clinical treatment.

2. Material and methods

2.1. Materials

In this study, gelatin, hydroxyphenylpropionicl acid, methyl acrylyl glycidyl, lithium phenyl-2,4,6-trimethylbenzoylphosphinate (LAP), kartogenin, atorvastatin and horse radish peroxidase were purchased from Sigma-Aldrich. All the other chemicals were reagent grade and deionized water was used.

2.2. Preparation and characterization of scaffolds

Gelatin-hydroxyphenylpropionicl acid (**GL-HP**) was synthesized according to a previously described method [32]. Briefly, 0.66 g Hydroxyphenylpropionic acid (HPA) was dissolved in 40 mL dimethyl sulfoxide (DMSO). After dissolution, 60 mL Milli-Q water was added. 0.64 g N, N-dimethylformamide (DMF) and 0.76 g 1-ethyl-3- (3-dimethylaminopropyl)-carbodiimide hydrochloride (EDC) were dissolved in the DMSO and water mixture above. The pH was adjusted between 4.5 and 5, and the carboxyl group was stirred at room temperature at high rotational speed for carboxyl group activation. After stirring for 3 h, pour 60 mL of 6.6 % (w/v) gelatin solution into the mixture and stir overnight at room temperature at a pH of 4.5–5. After the reaction was over, the above solution was transferred to a 10 kDa dialysis bag and dialyzed in Milli-Q for 3 days. Finally freeze-dried **GL-HP** can be stored at −20 °C. To prepare **GL-HP$_{KGN}$**, 10 mg KGN should be added along with HPA.

To prepare **GL-HP/GMA** [33], dissolving 2.5 g of **GL-HP** macromer in Milli-Q water (2 %, w/v), the pH of the solution was adjusted to 3.5 with 1 M HCl. After this, 10 mL of methyl acrylyl glycidyl (GMA) was added into the solustion at a rate of 0.5 mL/min. The reaction was conducted at 50 °C for 24 h and the product was purified by dialysis against Milli-Q water with the above-mentioned dialysis membrane at 40 °C for 7 days. The purified product was freeze-dried and stored at −20 °C for future use. To prepare **GL-HP/GMA$_{AT}$**, 66 mg AT should be added with HPA and GMA.

2.3. Hydrogel preparation

Unless otherwise stated, all concentrations are given as a percentage of weight per volume (w/v). **GL-HP** (50 mg, 5 wt%), **GL-GMA** (50 mg, 5 wt%) or **GL-HP/GMA** (50 mg, 5 wt%), and lithium acylphosphonate (LAP) (0.2 wt%) were dissolved in 1 mL PBS solution (pH 7.4)

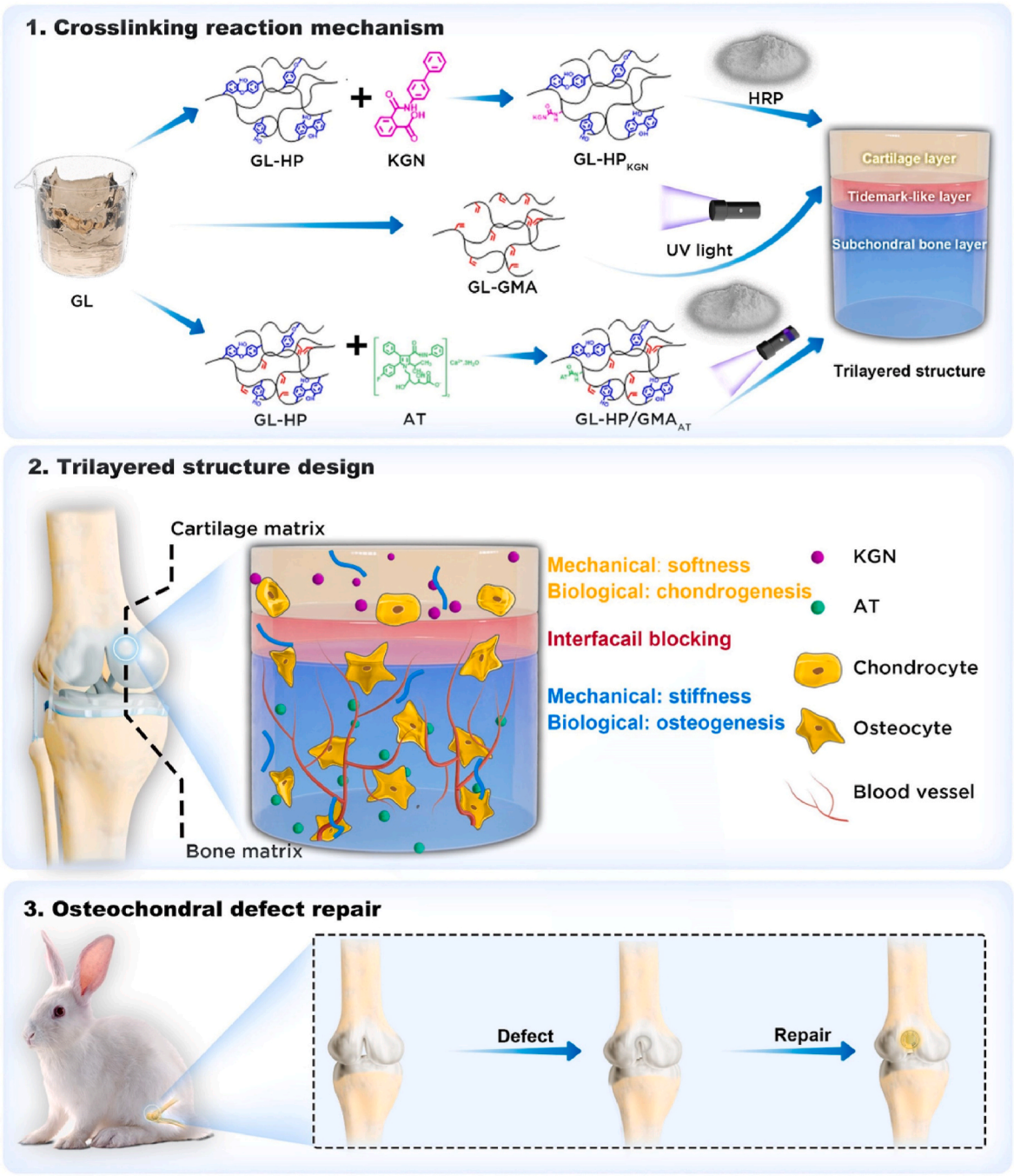

Fig. 1. Schematic illustration of the biomimetic design of trilayered hydrogel scaffolds with dual-differential microenvironment for articular osteochondral defect repair in rabbits.

respectively to obtain a trilayered hydrogel. All hydrogel formulations were fully mixed with continuous stirring, sterilized with a syringe filter (0.22 μm pore size). Finally, the hydrogel of **GL-HP** formulation was enzyme cross-linking was performed by 15 U/mL HRP and 0.85 mM/L H_2O_2 for 20–30 s [34]. The hydrogel of **GL-GMA** and **GL-HP/GMA** formulations were photo-crosslinked by exposure to blue light at the wave length of 365 nm using a light-emitting diode (LED) source (Uvata Precision Optoelectronics Co., Ltd.) with an intensity of 20 mW cm^{-2} for an exposed time of 5–10 s.

2.4. ^1H Nuclear magnetic resonance (NMR)

All the synthesized small molecules were confirmed by ^1H NMR according to the previously described method. ^1H NMR spectroscopy was acquired using Varian INOVA NMR spectrometer (Bruker, Billerica, MA, USA) with a uniaxial gradient inverse probe at a frequency of 300 MHz. Prior to measurement, 10 mg of the synthetic small molecule was dissolved in 1 mL of deuterium oxide containing 0.05 % (w/v) 3 - (trimethylsilver) propionic −2,2,3,3-d4 acid sodium salt (Sigma-Aldrich, St. Louis, Missouri, USA). Unfunctionalized raw gelatin was also tested as a control. The experiment was independently repeated three times.

2.5. Rheological analyses of hydrogels precursors

Dynamic rheology experiments were performed on the HAAKE MARS III photorheometer with parallel-plate (P20 TiL, 20 mm diameter)

geometry and OmniCure Series 2000 (365 nm, 20 mW cm^{-2}) at 25 °C. Time-sweep oscillatory tests were performed at a 10 % strain (CD mode), 1 Hz frequency, and a 0.5 mm gap for 180 s. Strain sweep oscillatory tests were performed to verify the linear response. The gel point was determined as the time when the storage modulus (G′) surpassed the loss modulus (G″). The final shear modulus was determined as the storage modulus (G′) reaching to the complete gelation. Temperature-sweep oscillatory tests were performed at 10 % strain (CD mode) and 1 Hz frequency parameters from 50 to 0 °C. The sol-to-gel transition point was determined as the time when the storage modulus (G′) surpassed the loss modulus (G″). Viscosity tests were performed at a gradual increasing shear rate from 0 to 50 s^{-1}.

2.6. Characterization by SEM

Hydrogel samples with different components were freeze-dried for 24 h and gold was sprayed on the longitudinal section with Quorum SC7620 sputtering coater for 45 s, followed by observation with a ZEISS GeminiSEM 300 scanning electron microscope at an accelerated voltage of 15 Kv.

2.7. Equilibrium porosity

The porosity (average void volume) of the hydrogel was determined using alcohol. All experiments were conducted in triplicate. Freeze-dried hydrogels were immersed in a sealed tube containing alcohol for 24 h, at which the weight of the sample (W_{24}) was constant. The actual volume (Va) of the sample was calculated using the following formula:

$$Va = (W_{24} - W_0) / p$$

Where W_{24} and W_0 are respectively the sample at 24 h and 0 h, and p is the density of alcohol (0.785 g/cm^3). The porosity was determined using the following equation:

$$Porosity\ (\%) = Va/Ve \times 100\%$$

Where Ve is the exterior volume of each sample.

2.8. Swelling and degradation tests

Swelling and enzymatic degradation of hydrogels were tested using gravimetric methods described in previous studies [35,36]. The cylindrical hydrogel samples (diameter = 10 mm; height = 2 mm) were recorded for the initial weights (W_0). For swelling tests, the hydrogels were fully immersed in PBS solution (pH = 7.4) for 24 h until complete swelling (n = 4). When the masses of these hydrogels became constant, the values were recorded as the wet weights (W_t). The swelling ratio was calculated according to Equation

$$Swelling\ Ratio\ (\%) = W_t/W_0 \times 100\%$$

For enzyme-mediated degradation tests, the above hydrogels after complete swelling were recorded for the initial weights (W_0). Then, the hydrogels were incubated in PBS (pH = 7.4) supplemented with 15 U mL^{-1} of collagenase for observing enzyme-mediated degradation at 37 °C (n = 4). The culture solution was refreshedevery day to maintain the enzyme activity. At each time point, these samples were carefully collected, and gently blotted with filter paper to remove excess water on the surfaces, and recorded for the residual weights (W_t). The degradation ratio (%) was calculated according to Equation

$$Degradation\ ratio\ (\%) = W_t/W_0 \times 100\%$$

2.9. Ultraviolet spectrum

The UV diffused reflection test (PE lambda 750) was used to set the wavelength in the range of 195–230 nm. **GL-KGN, GL-HP_{KGN}, GL-AT** and **GL-HP/GMA_{AT}** were added with PBS as the medium of 1 mL each. PBS was used as the blank group to determine the wave crest and observe whether the drug was successfully grafted. According to the absorption peak of the two drugs between 195 and 230 nm, the standard curve was made by measuring the concentration gradient of the drug at 200 nm wavelength, and the absorbance of GL-HP, GL-HP_{KGN} and GL-HP/GMA_{AT} were also measured at this wavelength and corresponding to the standard curve to calculate the graft rate of the drug. The grafting rate was calculated using the following formula:

$$Grafting\ rate\ (\%) = Wm/\ (Wm + Wq) \times 100\%$$

Where Wm is the grafted monomer mass and Wq is the graft monomer homopolymer quality.

2.10. Isolation and culture of rabbit BMSCs

BMSCs were obtained from the bone marrow of adult rabbist, and harvested, cultured, and expanded in the culture medium (Mesenchymal Stem Cell Medium, 7501, ScienCell), at 37 °C with 5 % CO_2 of incubator, medium was changed every two days to ensure sufficient nutrient supply to the cells. Cells were used previously reported when they expanded into the second generation [37].

2.11. Cytotoxicity tests

To determine the cytotoxicity of small molecule drugs KGN, AT and hydrogels, BMSCs were inoculated into 96 - well plates at a density of 2 × 10^3 cells/well, and then cultured *in vitro* for 1, 4, and 7 days after the cells were attached to the wall with different concentrations of solution to be tested. According to the manufacturer's instructions, use cell counting Kit-8 (CCK-8; Dojindo) measured cell proliferation and expressed it as an average optical density (OD) value for five wells, with each experiment repeated four times.

2.12. Cell viability, spreading, and migration assessment

The BMSCs of rabbits were mixed with five hydrogel groups (**GL-HP, GL-HP_{KGN}, GL-GMA, GL-HP/GMA** and **GL-HP/GMA_{AT}**; 5 × 10^6 cells/mL) were mixed, then injected into a cylindrical mold (10 mm diameter, 2 mm height) and rapidly polymerized for 60 s under light irradiation (365 nm, 20 mW/cm2) for about 5 s. The hydrogel structures containing BMSCs were incubated at 37 °C under 5 % CO_2 for 14 days. During *in vitro* culture, 2 mL of preheated osteogenic differentiation solution (OriCell™ Basal Medium For Cell Culture) was carefully and completely covered over each gel and replaced every 3 days. BMSCs-hydrogel constructs were cultured at days 0, 1, and 4. BMSCs activity in the gel was assessed by live/dead cell viability assays (Dojindo) and checked by CLSM (Leica, TCS SP8 STED 3X) as per manufacturer's instructions.

2.13. In vitro osteogenic, chondrogenic induction experiments

In order to verify the chondrogenic and osteogenic effects of small molecule drugs KGN and AT, rabbit BMSCs were implanted on 6 - well plates with 6 × 10^4 cells/well. After Cell adhesion, preheated Chondroblast Medium containing KGN and OriCellTM Basal Medium For Cell Culture containing AT were added to the pore plate, and replaced every three days during *in vitro* culture. After 14 days, the growth promoting effect was further determined by alizarin red (AR) staining. RT-qPCR was used to evaluate the effect of small molecule drugs on the expression of cartilage-related genes (*COL2, ACAN, SOX-9*) and bone-related genes (*OCN, BMP-2*) in BMSCs [38]. Detailed experiments were carried out according to the standard scheme. All experiments were conducted four times and using $2^{-\triangle\triangle CT}$ method. In addition, the rabbit BMSCs were co-cultured in the chondroblast or osteogenic induction

medium for 7 days, and then the cells were fixed by specific fluorescence staining COL2 or OCN.

2.14. Animal model of osteochondral defect

All animal models used in these studies were conducted according to standard guidelines approved by the Ethics Committee of Shanghai Jiao Tong University (#ZJU20170969). Adult male New Zealand white rabbits (2.5–3 kg) were used for *in vivo* studies. Under the anesthesia of 1 % pentobarbital sodium (40 mg/kg), cylindrical cartilage defects of osteochondral cartilage with a diameter of 5 mm and a depth of 4 mm were formed on the trochlear groove of the left and right limbs with trephine. Rabbits were randomly divided into three groups: untreated group (blank group), stent group (control group), and small molecule drug stent group (experimental group), with the number of repaired joints in each group greater than 8. Before disinfection and wound closure, the control and experimental stents were implanted in the defect groove, while the untreated group was simply sterilized and sutured. At 6 and 12 weeks after surgery, the rabbits were killed and histological evaluations were performed on eight knee joints in each group.

2.15. Micro-CT image analysis of bones

Briefly, samples were fixed with 4 % paraformaldehyde for 48 h. After image reconstruction, the desired region of interest with defects was assigned. The reconstructed images were then visualized and evaluated by Version 3.1 software provided by Shanghai Showbio (Biotech Co., Ltd, SKYSCAN 1076). Sample scanning related parameters are as follows: 70 kv (voltage), 200 μA (current), 30 μm (resolution), 300 ms (exposure time) [39].

2.16. Assessment of cartilage repair

At 6 and 12 weeks postoperatively, rabbits were killed by intravenous injection of an overdose of pentobarbital. According to the International Cartilage Repair Society (ICRS) macro assessment scale of cartilage repair, four different researchers collected, photographed and conducted blind evaluations from each group. Subsequently, continuous sections (5 mm thick) were made sagittal through the damaged site and stained with safranin O (Sigma). Four researchers used the ICRS Visual histological Assessment scale to blind score different groups of repaired cartilage.

2.17. Histological analysis

According to our previously established method, the collected samples were fixed, decalcified, embedded in paraffin wax and cut into 5 mm sections for histological and immunohistochemical analysis. Sections were stained with hematoxylin and eosin (H&E), safranin-O and fast green (SO/FG), and type II collagen (COL II, polyclonal antibody ab347121:10, Abcam, Cambridge, UK) to assess tissue structure and cartilage ECM deposition [40].

2.18. Statistical analysis

Data (n = 4) were expressed as the means ± standard deviations. A one-way analysis of the variance was used to determine the statistical significance of the difference between groups using Graph Pad Prism 7.00 software, and a p-value <0.05 was considered statistically significant.

3. Results

3.1. Preparation and characterization of dual-crosslinked hydrogels

In this study, gelatin by various amino acids through amino groups and carboxyl groups to form a polypeptide chain, *p*-hydroxyphenylpropionic acid mainly contains carboxyl, phenolic hydroxyl and double bond structure, methamphetamine glycerin has double bonds and epoxy groups.(2.3) The *p*-hydroxyphenylpropionic acid-grafted gelatin **(GL-HP)** conjugates were successfully synthesized by a carbodiimide/active ester-mediated coupling reaction [41], while the glycidyl methacrylate-grafted gelatin (**GL-GMA**) conjugates were successfully synthesized by an epoxy ring-opening addition reaction [42]. The *p*-hydroxyphenylpropionic acid/glycidyl methacrylate-grafted gelatin (**GL-HP/GMA**) conjugates were successfully synthesized by the above sequential grafting reactions (Fig. 2A). We chose gelatin among many hydrogels because of its high porosity, good biocompatibility and degradability. The ^{1}H NMR spectra further confirmed the successful grafting of HP (6.8–7.3 ppm) and GMA (5.5–6.2 ppm) groups on gelatin (Fig. 2C). To prepare the trilayered biomimetic hydrogel scaffolds, the single-crosslinked network of **GL-HP** hydrogels were prepared by HP-based enzyme crosslinking *via* two-component mixing, meanwhile the **GL-GMA** hydrogels were prepared by GMA-based photo-crosslinking upon light irradiation (365 nm LED, 20 mW cm^{-2}). Furthermore, the dual-crosslinked network of **GL-HP/GMA** hydrogels were quickly formed by means of both HP-based enzyme crosslinking and GMA-based photo-crosslinking reactions (Fig. 2B and D). The line chart of Fig. 2D further illustrates the gelation process of GL-HP/GMA hydrogels that G′ gradually surpassed G′′upon light irradiation."

To further investigate the physicochemical properties of hydrogels, the rheological analyses, SEM examination, and quantitative tests of porosity, swelling ratio, and degradation rate were performed respectively. As shown in Fig. 2E, the gel point of **GL-GMA** (3.7 ± 0.9 s) and **GL-HP/GMA** (6.3 ± 1.2 s) hydrogels were shorter than that of **GL-HP** (20.0 ± 5.0 s) hydrogels due to the rapid crosslinking rate of photopolymerization reaction. Additionally, the shear modulus of **GL-HP/GMA** (1500 ± Pa) hydrogels was stronger than those of **GL-HP** (70 ± Pa) and **GL-GMA** (700 ± Pa) hydrogels based on the formation of dual-crosslinked network (Fig. 2F). The SEM examination showed that each lyophilized hydrogel scaffolds displayed a highly interconnected and uniform pore microstructure (Fig. 3A). The porosity of lyophilized **GL-HP** (47.7 ± 1.8 %) hydrogels were smaller than those of lyophilized **GL-GMA** (61.4 ± 2.0 %) and **GL-HP/GMA** (59.5 ± 3.4 %) hydrogels, suggesting the significant difference in both hydrogel composition and crosslinking density (Fig. 3B). Moreover, the swelling ratio of the **GL-HP** (155.3 ± 12.1 %) hydrogels was larger than those of the **GL-GMA** (106.0 ± 12.4 %) and **GL-HP/GMA** (123.6 ± 11.9 %) hydrogels (Fig. 3C). The degradation rate of both the **GL-GMA** and **GL-HP/GMA** hydrogels in a collagenase solution was slower than that of the **GL-HP** hydrogels due to the relatively stable chemical bonds than the unstable physical bonds (Fig. 3D).

3.2. Characterization of drug-grafted functional hydrogels

To prepare drug-grafted functional hydrogels for cartilage and bone regeneration, the KGN-grafted **GL-HP** (**GL-HP$_{KGN}$**) and AT-grafted **GL-HP/GMA** (**GL-HP/GMA$_{AT}$**) conjugates were successfully synthesized, the grafting rate of KGN was 0.20 % and that of AT was 0.32 %. (Fig. 4A). The results of ultraviolet spectroscopy further verified the successful grafting of two drugs onto **GL-HP** and **GL-HP/GMA** conjugates respectively (Fig. 4B and C). Then, the physicochemical properties of **GL-HP$_{KGN}$** and **GL-HP/GMA$_{AT}$** hydrogels were also evaluated by the rheological analyses, SEM examination, and quantitative tests of porosity, swelling ratio, and degradation rate. As shown in Fig. 4D–F, the gel point of **GL-HP$_{KGN}$** hydrogels (33.0 ± 5.6 s) was relatively longer than that of **GL-HP/GMA$_{AT}$** hydrogels (5.9 ± 1.7 s). Meanwhile, the

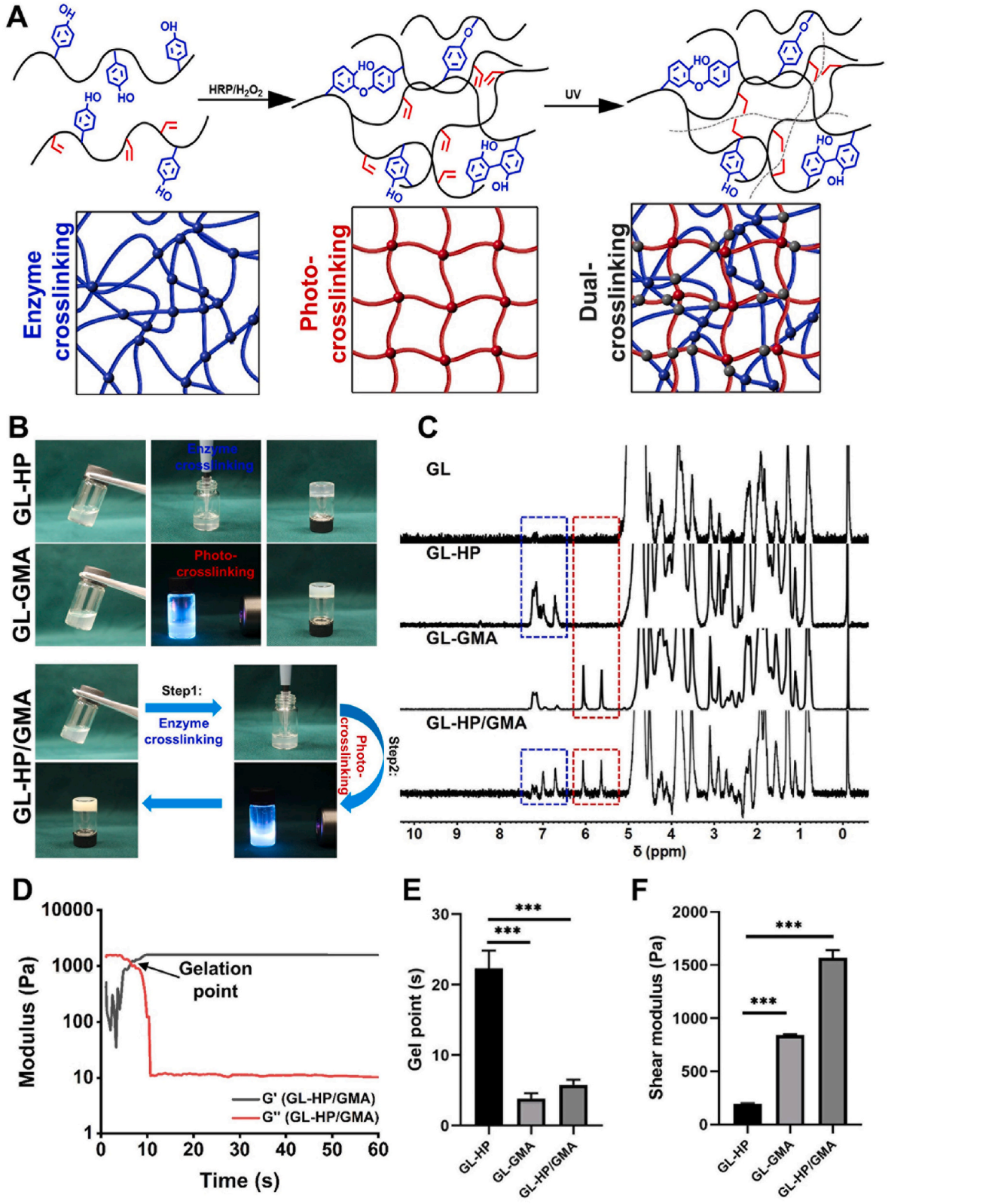

Fig. 2. Preparation and characterization of dual-crosslinked hydrogels. A) Schematic of the molecular formulas and dual-crosslinked network. Blue network represents enzyme crosslinking; red network represents photo-crosslinking. B) Photographs show the sol-to-gel transition of **GL-HP**, **GL-GMA**, and **GL-HP/GMA** hydrogels. C) ^{1}H NMR spectra demonstrate the successful grafting of *p*-hydroxyphenylpropionic acid (HP) and methyl glycidyl methacrylate (GMA) groups on gelatin. Blue dotted box represents HP groups; red dotted box represents GMA groups. D) Time-sweep rheological analysis of the **GL-HP/GMA** hydrogels. E, F) The statistical data of gel point (E) and shear modulus (F) of **GL-HP**, **GL-GMA**, and **GL-HP/GMA** hydrogels. ***$p < 0.001$. (For interpretation of the references to color in this figure legend, the reader is referred to the Web version of this article.)

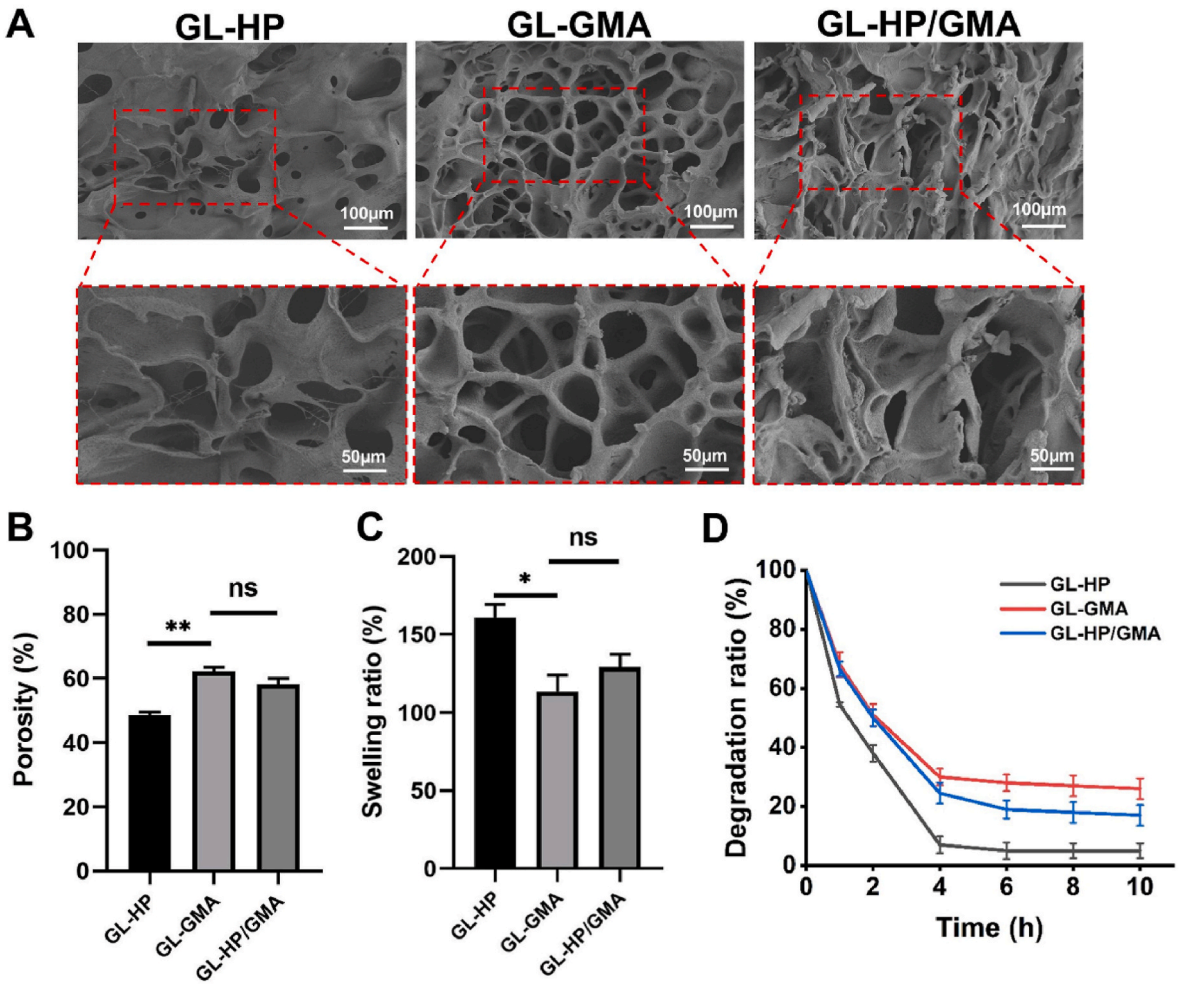

Fig. 3. The physicochemical properties of hydrogel structure, swelling ratio, and degradation rate. A) The SEM images of lyophilized **GL-HP, GL-GMA** and **GL-HP/GMA** hydrogel scaffolds. B) The open porosity of lyophilized hydrogels with different components. C) The swelling ratio of **GL-HP, GL-GMA** and **GL-HP/GMA** hydrogels. D) The degradation rate of **GL-HP, GL-GMA** and **GL-HP/GMA** hydrogels in the collagenase solution (0.15 U/mL). $*p < 0.05$, $**p < 0.01$, ns = no significance.

shear modulus of **GL-HP/GMA$_{AT}$** hydrogels (668.2 ± 6.9 Pa) was significantly higher than that of **GL-HP$_{KGN}$** hydrogels (54.4 ± 1.2 Pa), which is suitable for the construction of tissue-specific differential mechanical microenvironment. Moreover, the porosity of lyophilized **GL-HP$_{KGN}$** hydrogels (66.9 ± 11.8 %) was slightly higher than that of lyophilized **GL-HP/GMA$_{AT}$** hydrogels (52.2 ± 11.6 %) (Fig. 4G). The swelling ratio of **GL-HP$_{KGN}$** hydrogels had no significant difference on **GL-HP/GMA$_{AT}$** hydrogels (Fig. 4H). Additionally, both **GL-HP$_{KGN}$** and **GL-HP/GMA$_{AT}$** hydrogels could be easily degraded in a collagenase solution due to the biodegradable characteristic of gelatin (Fig. 4I). All these results demonstrate that the tissue-specific hydrogels are considered as promising tissue-engineered scaffolds because of the suitable rheological and mechanical properties, as well as reasonable swelling ratio and degradation rate.

3.3. Biological function evaluation of the tissue-specific hydrogels

To evaluate the biological function of drug-grafted functional hydrogels, the cytocompatibility of both KGN and AT drugs was firstly assessed using the CCK-8 assay. As shown in Fig. 5A and C, after incubating either KGN or AT drugs with BMSCs in the range of 0.1–100 μM, cells still show good viability. Then, the suitable drug concentration of 10 and 50 μM or 1 and 10 μM was selected for 1, 4, and 7 days of BMSC co-incubation, further confirming that there was no significant effect on cell proliferation (Fig. 5B and D). To investigate the biological function of corresponding drugs, the immunofluorescence staining and real-time polymerase chain reaction (RT-PCR) analyses were performed. As shown in Fig. 5E and G, the cartilage-specific protein COL2 expression was obviously increased in the W/KGN (with KGN) groups, which was further confirmed by the upregulated expression of chondrogenic genes of *COL2*, *ACAN*, and *SOX-9*. Additionally, the bone-specific protein OCN expression and the calcium salt deposition of alizarin red staining were significantly increased in the W/AT (with AT) groups (Fig. 5E and F), which was also confirmed by the upregulated expression of osteogenic genes of *OCN* and *BMP-2* (Fig. 5H). Historically, statins were primarily utilized for cardiovascular conditions, with some research focusing on their impact on bone defect repair by inhibiting osteoclast-related gene expression. In this study, at a concentration of 1 μM, atorvastatin (AT) significantly up-regulated the expression of osteocalcin (OCN), a key gene in osteogenesis, by as much as 600 times. Furthermore, at 10 μM, AT also enhanced bone gene expression, although higher concentrations showed a diminishing effect on osteogenic function, warranting additional investigation.

Next, the cytocompatibility and tissue-specific induction of drug-grafted hydrogels were further investigated. As shown in Fig. 6A and C, the qualitative and quantitative results of live/dead fluorescence staining demonstrated that both drug-free (**GL-HP**, **GL-GMA**, and **GL-HP/GMA** hydrogels) and drug-grafted (**GL-HP$_{KGN}$** and **GL-HP/GMA$_{AT}$** hydrogels) groups had positive effect on BMSC survival and proliferation, indicating that there was no significant influence when the grafting

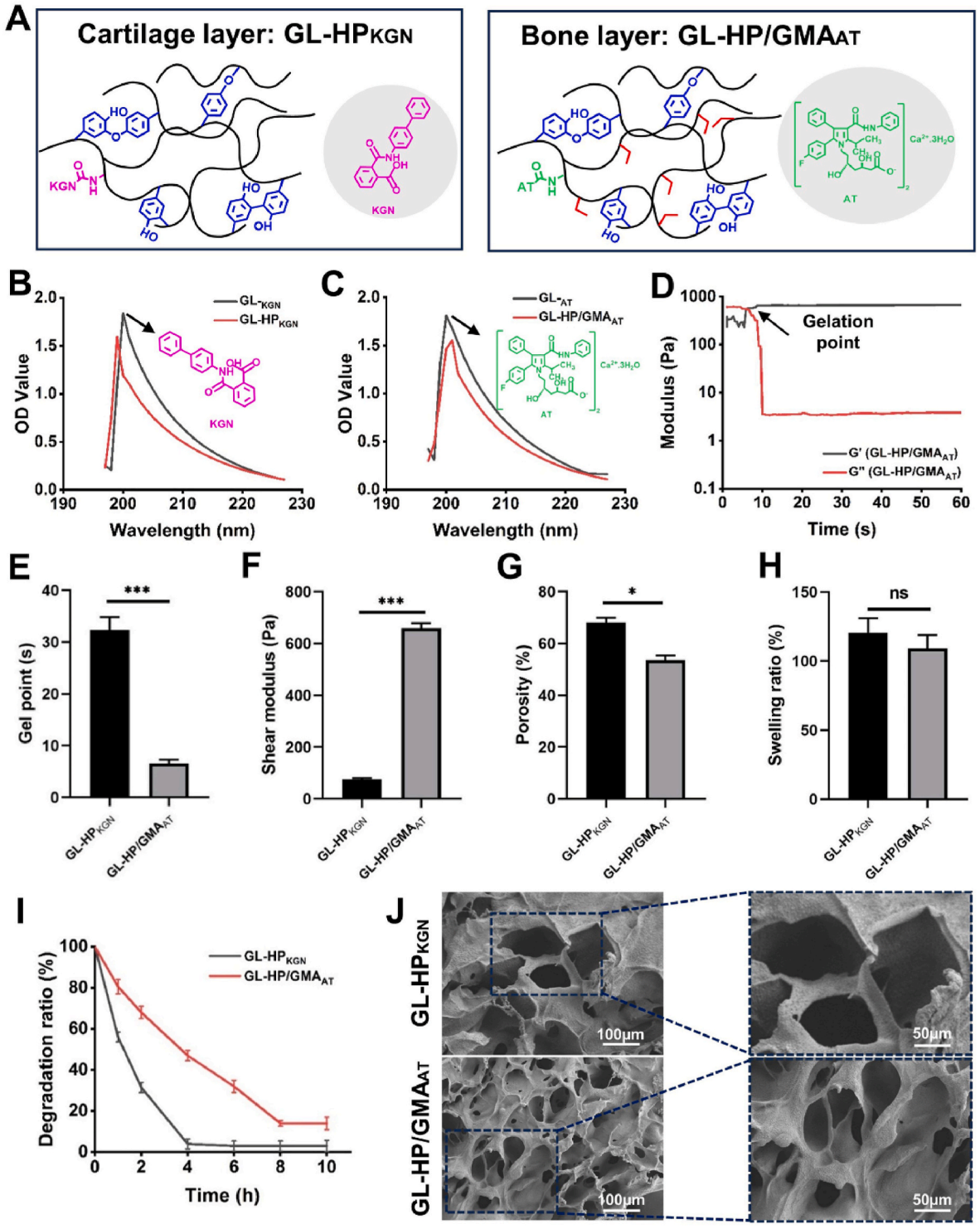

Fig. 4. Characterization of drug-grafted functional hydrogels. A) Schematic of the molecular formulas showing the cartilage layer consisted of **GL-HP$_{KGN}$** hydrogels and the bone layer consisted of **GL-HP/GMA$_{AT}$** hydrogels. B, C) The ultraviolet spectroscopy of the highest absorption peak exhibits the grafting drugs of **GL-HP$_{KGN}$** (B) and **GL-HP/GMA$_{AT}$** (C) biomacromolecules. D) Time-sweep rheological analysis of the **GL-HP/GMA$_{AT}$** hydrogels. E-H) The statistical data of gelation time (E), shear modulus (F), open porosity (G), and swelling ratio (H) of both **GL-HP$_{KGN}$** and **GL-HP/GMA$_{AT}$** hydrogels. I) The degradation rate of both **GL-HP$_{KGN}$** and **GL-HP/GMA$_{AT}$** hydrogels in the collagenase solution (0.15 U/mL). J) The SEM images of lyophilized **GL-HP$_{KGN}$** and **GL-HP/GMA$_{AT}$** hydrogel scaffolds. $^{*}p < 0.05$, $^{***}p < 0.001$, ns = no significance.

of drugs onto hydrogels. Moreover, good cell viability also verified by CCK-8 assay for the extracts of the corresponding drug-grafted hydrogels (Fig. 6B). The RT-PCR results further confirmed that the chondrogenic genes of *COL2*, *ACAN*, and *SOX-9*, as well as the osteogenic genes of *OCN* and *BMP-2* were respectively upregulated when co-cultured with the degraded products of **GL-HP$_{KGN}$** and **GL-HP/GMA$_{AT}$** hydrogels (Fig. 6D and E), consistent with the results of drugs as shown in Fig. 5G and H.

All these results demonstrate that the drug-grafted tissue-specific hydrogels not only have good cytocompatibility, but also effectively promote the chondrogenic and osteogenic differentiation of BMSCs.

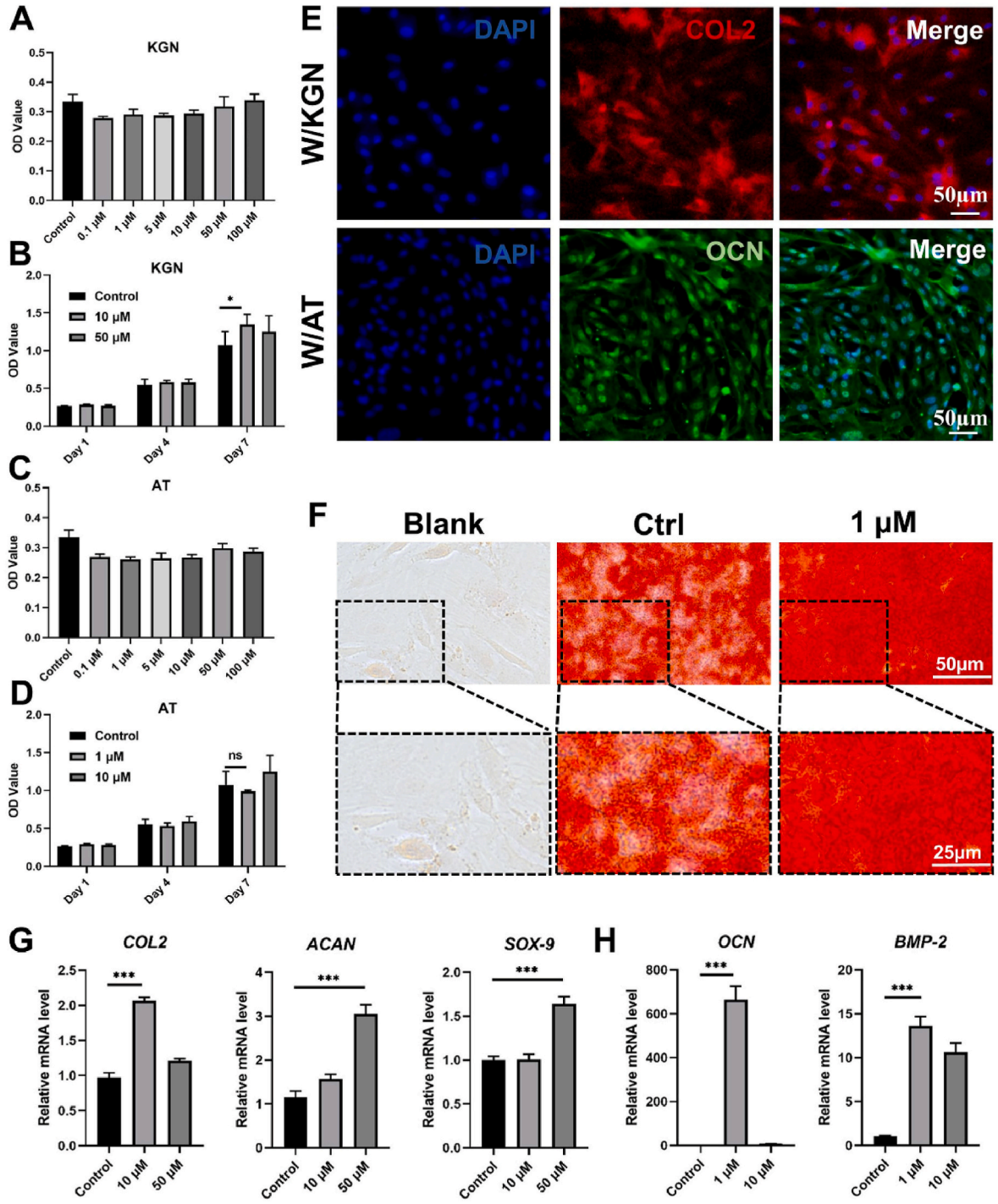

Fig. 5. Biological function evaluation of drugs for chondrogenic and osteogenic differentiation. A, C) The CCK-8 assay of KGN (A) and AT (C) drugs at different concentrations from 0.1 to 100 μM shows satisfactory cytocompatibility on day 1. B, D) The CCK-8 assay of 10 μM and 50 μM KGN (B) 1 μM and 10 μM AT (D) drugs on days 1, 4, and 7 shows good proliferation of BMSCs. E) Immunofluorescence staining of COL2 (red) and OCN (green) with the addition of KGN and AT drugs respectively. F) The alizarin red staining shows the calcium salt deposition in different groups. Blank group represents BMSCs in culture medium; Ctrl group represents BMSCs with osteogenic induction medium; 1 μM group represents BMSCs with osteogenic induction medium and 1 μM AT drugs. G) Expression of cartilage-specific genes (*COL2*, *ACAN*, and *SOX-9*) induced by KGN drugs. H) Expression of bone-specific genes (*OCN* and *BMP-2*) induced by AT drugs. $*p < 0.05$, $***p < 0.001$, ns = no significance. (For interpretation of the references to color in this figure legend, the reader is referred to the Web version of this article.)

3.4. In vivo articular osteochondral defect repair using trilayered scaffolds

In this study, the trilayered biomimetic hydrogel scaffolds with dual-differential microenvironment were prepared by sequential crosslinking procedures as shown in Fig. 7A: the lower subchondral bone layer was constructed by **GL-HP/GMA$_{AT}$** hydrogels; the tidemark-like middle layer was constructed by **GL-GMA** hydrogels; the upper cartilage layer was constructed by **GL-HP$_{KGN}$** hydrogels. To investigate the repair effect of trilayered biomimetic hydrogel scaffolds, the cylindrical articular osteochondral defect models (5 mm in diameter, 4 mm in depth) were created in rabbits. The contrastive experiments were divided as three

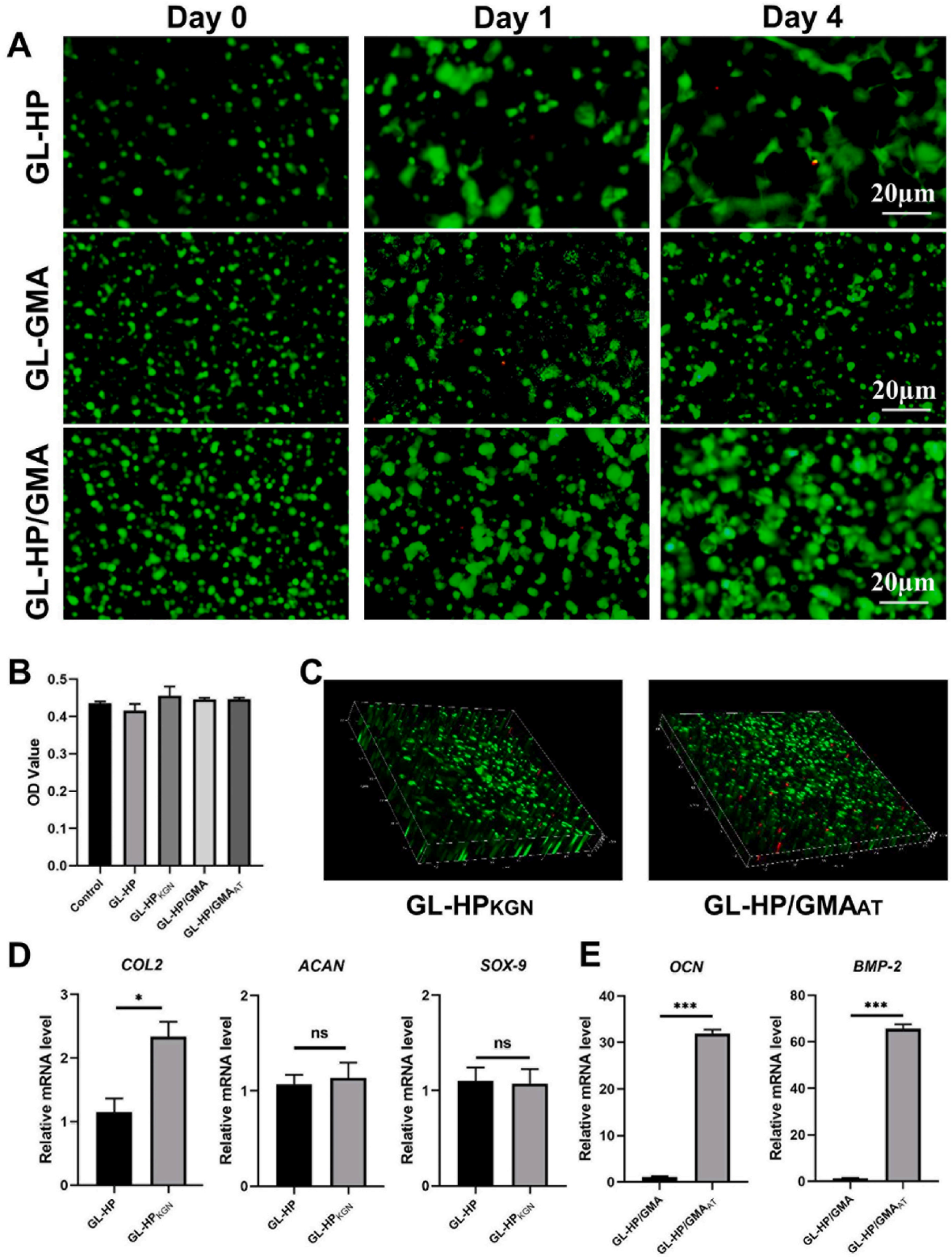

Fig. 6. Biological function evaluation of the tissue-specific hydrogels. A) The live/dead fluorescence staining of encapsulated BMSCs in **GL-HP**, **GL-GMA**, and **GL-HP/GMA** hydrogels on days 0, 1, and 4. B) The CCK-8 assay was detected by the co-culture of BMSCs with the extracts of **GL-HP**, **GL-HP$_{KGN}$**, **GL-GMA**, **GL-HP/GMA**, and **GL-HP/GMA$_{AT}$** hydrogels. C) The live/dead fluorescence staining of encapsulated BMSCs in **GL-HP$_{KGN}$** and **GL-HP/GMA$_{AT}$** hydrogels on days 7. D) Expression of cartilage-specific genes (*COL2*, *ACAN*, and *SOX-9*) of BMSCs co-cultured with the degraded product of **GL-HP$_{KGN}$** hydrogels. E) Expression of bone-specific genes (*OCN* and *BMP-2*) of BMSCs co-cultured with the degraded product of **GL-HP/GMA$_{AT}$** hydrogels. $^{*}p < 0.05$, $^{***}p < 0.001$, ns = no significance.

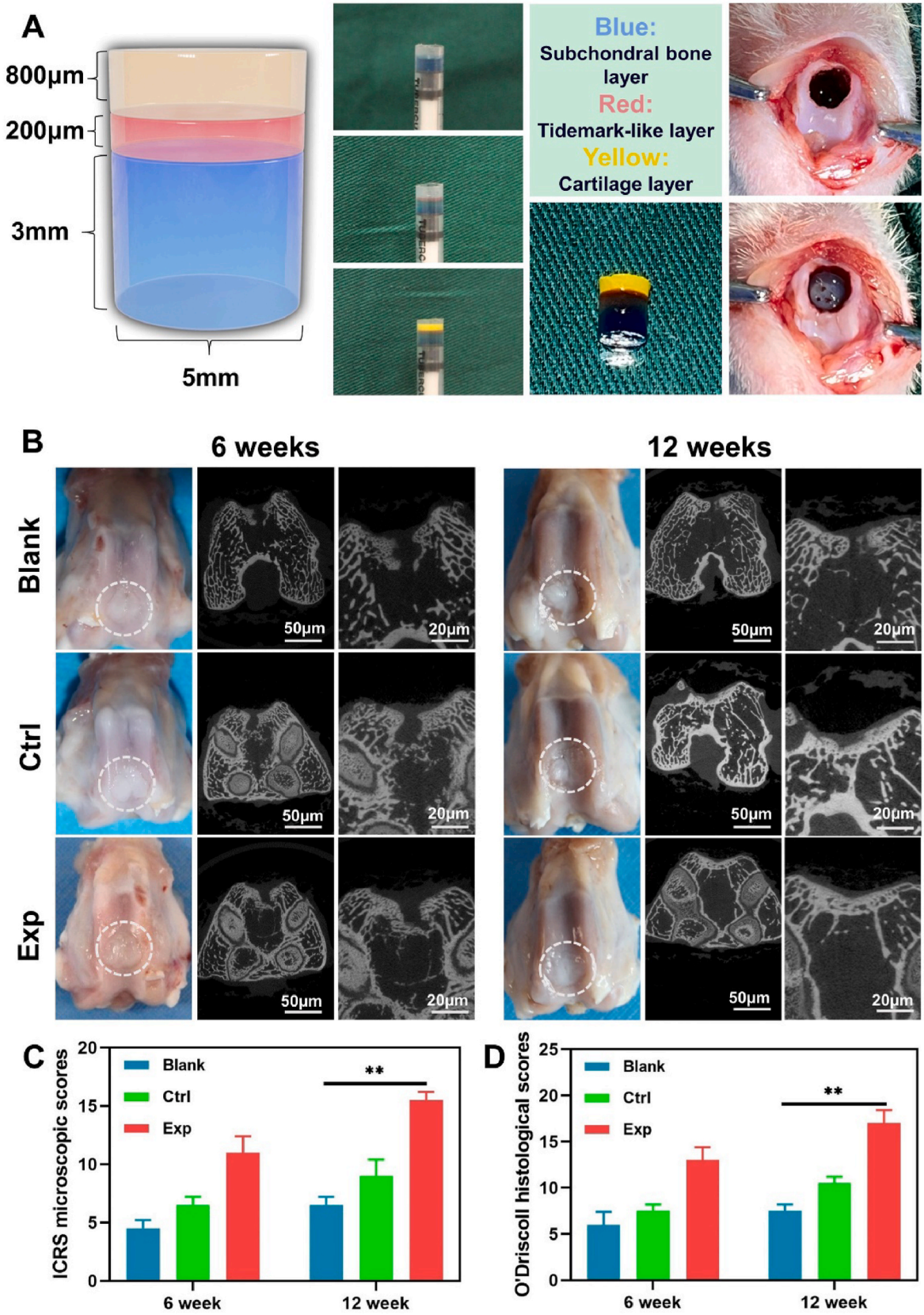

Fig. 7. Gross morphology, Micro-CT, and scores of samples at 6 and 12 weeks post-surgery. A) The design and photographs of trilayered biomimetic hydrogel scaffolds, as well as the articular osteochondral defect models of rabbits repaired by the trilayered scaffolds. Yellow represents the upper cartilage layer; red represents the tidemark-like middle layer; blue represents the lower subchondral bone layer. B) Gross views and Micro-CT images of the cross-section of coronal (upper) and sagittal (bottom) planes of the articular reconstructed regions. C, D) International Cartilage Repair Society (ICRS, C) and Modified O'Driscoll histology scoring system (MODS, D) scores of samples at 6 and 12 weeks post-surgery. $^{**}p < 0.01$. (For interpretation of the references to color in this figure legend, the reader is referred to the Web version of this article.)

groups: *i*) trilayered hydrogel scaffolds (**GL-HP$_{KGN}$ + GL-GMA + GL-HP/GMA$_{AT}$**) as experimental (Exp) groups; *ii*) trilayered hydrogel scaffolds (**GL-HP + GL-GMA + GL-HP/GMA**) as control (Ctrl) groups; *iii*) untreated defects as blank groups.

The rabbits were sacrificed and collected for gross observation, Micro-CT, and histological examinations at 6 and 12 weeks post-surgery. In the Ctrl group, the osteochondral defects were filled with white and soft fibrous-like tissue in the articular surface. However, the reconstructed osteochondral tissue in the Exp group was relatively mature and showed the seamless interfacial integration, which was similar to the normal articular tissue (Fig. 7B). Moreover, the Micro-CT results demonstrated that all the groups of subchondral bone layers underwent a gradual ossification process from 6 weeks to 12 weeks. Noticeably, the Exp group showed an initial cylindrical defect at 6 weeks and repaired by intact cancellous bone at 12 weeks. The histological examinations of H&E, SO/FG, and Masson, as well as immunofluorescence staining of COL2 and OCN further confirmed the above observation (Fig. 8). In the Exp group, the cartilage defect region was successfully repaired by mature hyaline cartilage with typical lacuna structure and cartilage-specific matrix deposition that verified by positive staining of safranin-O and COL2, while the bone defect region was successfully repaired by mature cancellous bone with typical trabecular structure

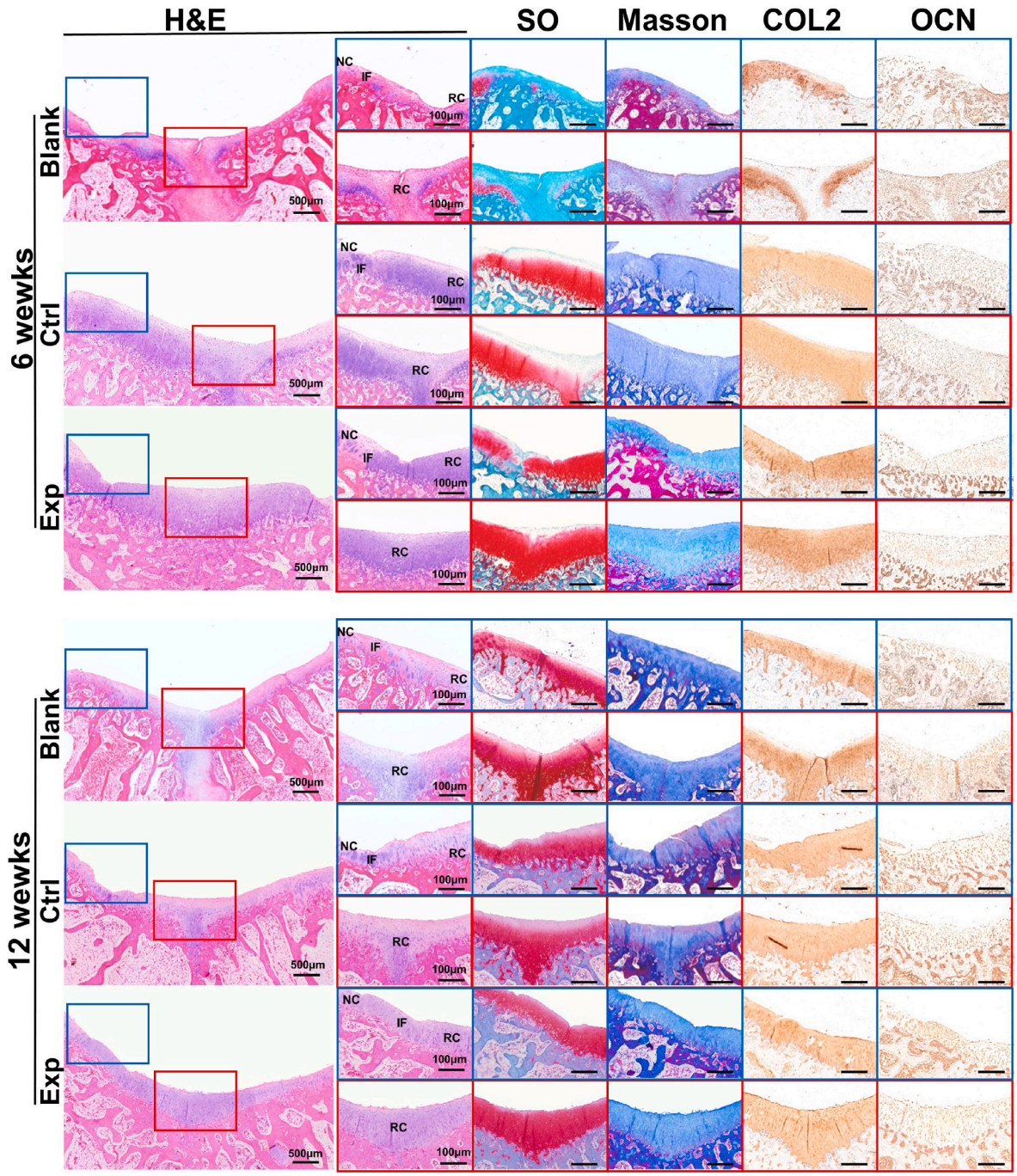

Fig. 8. Histological examinations of samples at 6 and 12 weeks post-surgery. Representative histological staining of H&E, safranin-O/fast green, and Masson's trichrome, as well as immunofluorescence staining of COL2 and OCN of the osteochondral defect regions of Blank, Control (Ctrl), and Experimental (Exp) groups at 6 and 12 weeks post-surgery. RC: repaired cartilage; IF: interface; NC: native cartilage. (For interpretation of the references to color in this figure legend, the reader is referred to the Web version of this article.)

and bone-specific matrix deposition that verified by positive staining of Masson, fast green, and OCN. Importantly, the clear tidemark-like structure close to the surrounding native tissue could be observed between the regenerated cartilage and bone regions, confirming the necessary structural design of the tidemark-like middle layer. Consistent with the above observation, both blank and Ctrl groups had dissatisfactory repair in both the cartilage and bone defect regions. Furthermore, both International Cartilage Repair Society (ICRS) and Modified O'Driscoll histology scoring system (MODS) scores of the Exp group were significantly higher than those of other two groups, indicating the articular osteochondral defects were more effective by means of the tissue-specific drug-grafted trilayered biomimetic hydrogel scaffolds (Fig. 7C and D).

4. Discussion

In the current study, we developed the trilayered biomimetic hydrogel scaffolds with dual-differential microenvironment for articular osteochondral defect repair. The upper cartilage layer was constructed by KGN-grafted **GL-HP$_{KGN}$** hydrogels *via* HP-based enzyme crosslinking reaction, while the lower subchondral bone layer was constructed by AT-grafted **GL-HP/GMA$_{AT}$** hydrogels *via* dual-crosslinked network of both HP-based enzyme crosslinking and GMA-based photo-crosslinking reactions. Additionally, the introduction of tidemark-like middle layer is conducive to the formation of well-defined cartilage-bone integrated architecture. The *in vitro* experiments demonstrated the significant mechanical difference of three layers, successful grafting of drugs, good cytocompatibility and tissue-specific induced function. Finally, the articular osteochondral defects were successfully repaired using the trilayered biomimetic hydrogel scaffolds by the activation of endogenous recovery, which offers a promising alternative for future clinical treatment.

How to prepare the tissue-specific hydrogels for both cartilage and bone regeneration with dual-differential microenvironment of mechanical and biological factors is the first challenge that we faced [43]. To address the above issue, we firstly fabricated the single- and dual-crosslinked hydrogels to provide the gradient mechanical microenvironment for cartilage and subchondral bone layers respectively. Meanwhile, the grafting strategy of small molecular drugs [44] was adopted to better mimic the tissue-specific biological microenvironment. In the current study, the upper cartilage layer was successfully constructed by signal-crosslinked **GL-HP$_{KGN}$** hydrogels, showing a soft and dynamical network with chondrogenic induced function for cartilage regeneration. The lower subchondral bone layer was successfully constructed by dual-crosslinked **GL-HP/GMA$_{AT}$** hydrogels, showing a stiff and mechanically stable network with osteogenic induced function for bone regeneration. The current results demonstrated that the gelation time of **GL-HP$_{KGN}$** hydrogels was approximately 20 s and the elastic modulus is only 70 Pa, whereas **GL-HP/GMA$_{AT}$** hydrogels only needed 5 s of light irradiation and exhibited a relatively high elastic modulus of approximately 700 Pa. Additionally, the drug carrying in hydrogel scaffolds was realized by stable chemical grafting *via* amidation reaction, while the sustained release of drugs from gelatin-based hydrogels was realized by the enzyme-mediated degradation of gelatin biomacromolecule. *In vitro* experiments further confirmed that the chondrogenic genes (*COL2*, *ACAN*, and *SOX-9*) were significantly increased upon the effect of released KGN drugs, while the osteogenic genes (*OCN* and *BMP-2*) were dramatically increased upon the impact of released AT drugs (*OCN* expression was up to about 600 times when the concentration of AT was 1 μM). All these results demonstrated that both the gradient mechanical strength and the tissue-specific biological microenvironment were conveniently regulated in hydrogel scaffolds.

Whether the trilayered biomimetic hydrogel scaffolds could repair articular osteochondral defects is the current pre-clinical consideration. Inspired by the physiological structure of native articular osteochondral tissue [45],we adopted the trilayered biomimetic architecture of upper cartilage layer, middle tidemark-like layer, and lower subchondral bone layer. In fact, the tidemark-like zone, as the calcification front of bone layer, plays an essential role in promoting interfacial integration and preventing blood vessels from invading into the cartilage layer [46]. In this study, the photocrosslinked **GL-GMA** hydrogels were chosen as the middle layer because of the dense crosslinked network to effectively withstand the infiltration of blood vessels. The current results demonstrated that the articular osteochondral defects of rabbit models were successfully repaired using the trilayered biomimetic hydrogel scaffolds by the activation of endogenous recovery. Compared with the use of exogenous stem cells, the endogenous repair based on bioactive scaffolds has the advantage of reducing the risk of immune rejection reaction [47]. Noticeably, the stable cartilage phenotype with typical cartilage lacuna was still maintained after 12-weeks surgery due to the effect of released KGN from **GL-HP$_{KGN}$** hydrogels, while the endochondral ossification was proceeded in the subchondral bone layer dependent on the osteogenic function of released AT from **GL-HP/GMA$_{AT}$** hydrogels. Furthermore, the boundary between the cartilage layer and the bone layer in the experimental group was clearly defined, indicating that the tidemark-like structural design is conducive to interfacial separation and tissue integration. It also needs to be pointed that the existence of cartilage layer collapse is due to the larger size of the osteochondral defects (diameter = 5 mm) that the repair rate could not keep up with the scope of the defects.

5. Conclusions

In summary, we proposed a novel strategy of trilayered biomimetic hydrogel scaffolds with dual-differential microenvironment for articular osteochondral defect repair. Firstly, the hardness gradient of hydrogel scaffolds was successfully adjusted by the crosslinked network, and thus regulated the differential mechanical microenvironment. Then, the released KGN and AT from gelatin-based hydrogels successfully promoted chondrogenic differentiation and osteogenic differentiation respectively, achieving the regulation of tissue-specific induced microenvironment. Finally, the articular osteochondral defects were successfully repaired using the trilayered biomimetic hydrogel scaffolds by the activation of endogenous recovery. Although there are still some problems to be further investigated in future, such as the prolonged repair period in large animal models, this study represents a proof-of-concept study for future articular osteochondral defect treatment.

Compliance with ethics guidelines

All authors (Hongying Chen, Jinyi Huang, Xiaomeng Li, Weiwei Zhao, Yujie Hua, Zhenfeng Song, Xianwei Wang, Guangdong Zhou, Zhikun Guo, Wenjie Ren and Yongkun Sun) declare that they have no conflict of interest or financial conflicts to disclose.

CRediT authorship contribution statement

Hongying Chen: Writing – original draft, Visualization, Software, Resources, Methodology, Investigation, Formal analysis, Data curation, Conceptualization. **Jinyi Huang:** Visualization, Methodology. **Xiaomeng Li:** Conceptualization, Investigation. **Weiwei Zhao:** Data curation. **Yujie Hua:** Writing – review & editing, Conceptualization, Project administration. **Zhenfeng Song:** Project administration. **Xianwei Wang:** Funding acquisition. **Zhikun Guo:** Funding acquisition. **Guangdong Zhou:** Writing – review & editing, Funding acquisition. **Wenjie Ren:** Supervision, Funding acquisition. **Yongkun Sun:** Writing – review & editing, Funding acquisition, Conceptualization.

Declaration of competing interest

The authors declare no competing interests.

Data availability

Data will be made available on request.

Acknowledgments

H.C., J.H., and X.L. contributed equally to this work. This research was financially supported by the National Key R&D Program Grant (2018YFC1105800), Open Project of the Third Affiliated Hospital of Xinxiang Medical University (KFKTZD202106), Henan Key Laboratory of Medical and Protective Products (YDFH2023KF06), Open Program of Henan Joint International Research Laboratory of Stem Cell Medicine (KFKT202105), Biomaterials and Regenerative Medicine Institute Cooperative Research Project of Shanghai Jiaotong University School of Medicine (2022LHA07), the Key Research and Development Program of Henan Province (221111310100), Shanghai Municipal Key Clinical Specialty (shslczdzk06601).

Appendix A. Supplementary data

Supplementary data to this article can be found online at https://doi.org/10.1016/j.mtbio.2024.101051.

References

[1] M. Cucchiarini, H. Madry, Biomaterial-guided delivery of gene vectors for targeted articular cartilage repair, Nat. Rev. Rheumatol. 15 (2019) 18–29. http://s41584-018-0125-2.
[2] J. Wu, L. Kuang, C. Chen, J. Yang, W. Zeng, T. Li, miR-100-5p-abundant exosomes derived from infrapatellar fat pad MSCs protect articular cartilage and ameliorate gait abnormalities via inhibition of mTOR in osteoarthritis, Biomaterials 206 (2019) 87–100. http://10.1016/j.biomaterials.2019.03.022.
[3] W. Lin, M. Kluzek, N. Iuster, Cartilage-inspired, lipid-based boundary-lubricated hydrogels, Science 370 (2020) 335–338. http://10.1126/science.aay8276.
[4] C. Lesage, M. Lafont, P. Guihard, P. Weiss, J. Guicheux, V. Delplace, Material-assisted strategies for osteochondral defect repair, Adv. Sci. 9 (2022). http://10.1002/advs.202200050.
[5] L. Zhou, V.O. Gjvm, J. Malda, Innovative tissue-engineered strategies for osteochondral defect repair and regeneration: current progress and challenges, Adv. Healthcare Mater. 26 (2020). http://10.1002/adhm.202001008.
[6] S. Wang, S. Zhao, J. Yu, Z. Gu, Y. Zhang, Advances in translational 3D printing for cartilage, Bone, and Osteochondral Tissue Engineering, Small 18 (2022). http://10.1002/smll.202201869.
[7] D. Kim, H. Cho, M. Thangavelu, J. Int, Osteochondral and bone tissue engineering scaffold prepared from Gallus var domesticus derived demineralized bone powder combined with gellan gum for medical application, Int. J. Biol. Macromol. 149 (2020) 381–394. http://10.1016/j.ijbiomac.2020.01.191.
[8] W. Wei, H. Dai, Articular cartilage and osteochondral tissue engineering techniques: recent advances and challenges, Bioact. Mater. 6 (2021) 4830–4855. http://10.1016/j.bioactmat.2021.05.011.
[9] J. Liao, T. Tian, S. Shi, The fabrication of biomimetic biphasic CAN-PAC hydrogel with a seamless interfacial layer applied in osteochondral defect repair, Bone Res 5 (2017). http://10.1038/boneres.2017.18.
[10] W. Hu, Y. Chen, C. Dou, S. Dong, Microenvironment in subchondral bone: predominant regulator for the treatment of osteoarthritis, Ann. Rheum. Dis. 80 (2021). http://10.1136/annrheumdis-2020-218089.
[11] H. Zhang, L. Wang, J. Cui, Maintaining hypoxia environment of subchondral bone alleviates osteoarthritis progression, Sci. Adv. 9 (2023). http://10.1126/sciadv.abo7868.
[12] W. Su, G. Liu, X. Liu, Angiogenesis stimulated by elevated PDGF-BB in subchondral bone contributes to osteoarthritis development, JCI Insight 5 (2020). http://10.1172/jci.insight.135446.
[13] H. Li, Z. He, W. Li, Exploring the mechanism of microfracture in the treatment of porcine full-thickness cartilage defect, Am. J. Sports Med. 51 (2023) 1033–1046. http://10.1177/03635465231153630.
[14] N. Li, J. Song, G. Zhu, Periosteum tissue engineering-a review, Biomater. Sci. 4 (2016) 1554–1561. http://10.1039/c6bm00481d.
[15] A. Ghouri, S. Muzumdar, A. Barr, E. Robinson, C. Murdoch, S. Kingsbury, P. Conaghan, The relationship between meniscal pathologies, cartilage loss, joint replacement and pain in knee osteoarthritis: a systematic review, Osteoarthritis Cartilage 30 (2022) 1287–1327. http://10.1016/j.joca.2022.08.002.
[16] H. Kwon, W. Brown, C. Lee, Surgical and tissue engineering strategies for articular cartilage and meniscus repair, Nat. Rev. Rheumatol. 15 (2019) 550–570. http://10.1038/s41584-019-0255-1.
[17] A.C. Daly, F.E. Freeman, T. Gonzalez-Fernandez, S.E. Critchley, J. Nulty, D.J. Kelly DJ, 3D bioprinting for cartilage and osteochondral tissue engineering, Adv. Healthcare Mater. 6 (2017). http://10.1002/adhm.201700298.
[18] C. Bertsch, H. Maréchal, V. Gribova, Biomimetic bilayered scaffolds for tissue engineering: from current design strategies to medical applications, Adv. Healthcare Mater. 12 (2023). http://10.1002/adhm.202203115.
[19] J. Xu, J. Ji, J. Jiao, 3D printing for bone-cartilage interface regeneration, Front. Bioeng. Biotechnol. 10 (2022). http://10.3389/fbioe.2022.828921.
[20] Z. Lv, P. Wang, W. Li, Bifunctional TRPV1 Targeted Magnetothermal Switch to Attenuate Osteoarthritis Progression, Wash D C), Research, 2024. http://10.34133/research.0316.) 7 0316.
[21] A. Armiento, A. Stoddart, M. Alini, D. Eglin, Biomaterials for articular cartilage tissue engineering: learning from biology, Acta Biomater. 65 (2018) 1–20. http://10.1016/j.actbio.2017.11.021.
[22] M. Castilho, V. Mouser, M. Chen, J. Malda, K. Ito, Bi-layered micro-fibre reinforced hydrogels for articular cartilage regeneration, Acta Biomater. 95 (2019) 297–306. http://10.1016/j.actbio.2019.06.030.
[23] F. Gao, Z. Xu, Q. Liang, Osteochondral regeneration with 3D-printed biodegradable high-strength supramolecular polymer reinforced-gelatin hydrogel scaffolds, Adv. Sci. 6 (2019). http://10.1002/advs.201900867.
[24] L. Gu, T. Shan, Y. Ma, F. Tay, L. Niu, Novel biomedical applications of crosslinked collagen, Trends Biotechnol. 37 (2019) 464–491. http://10.1016/j.tibtech.2018.10.007.
[25] J. Zhou, H. Wang, H. Chen, pH-responsive nanocomposite hydrogel for simultaneous prevention of postoperative adhesion and tumor recurrence, Acta Biomater. 158 (2023) 228–238. http://10.1016/j.actbio.2022.12.025.
[26] X. Wang, Q. Wang, Enzyme-Laden bioactive hydrogel for biocatalytic monitoring and regulation, Acc. Chem. Res. 54 (2021) 1274–1287. http://10.1021/acs.accounts.0c00832.
[27] S.U. Aydemir, Z. Kocer, I. Sahin, B. Aru, Oxidized regenerated cellulose cross-linked gelatin microparticles for rapid and biocompatible hemostasis: a versatile cross-linking agent, Carbohydr. Polym. 200 (2018) 624–632. http://10.1016/j.carbpol.2018.07.074.
[28] B.J. Klotz, D. Gawlitta, A.J. Rosenberg, J. Malda, F.P. Melchels, Gelatin-methacryloyl hydrogels: towards biofabrication-based tissue repair, Trends Biotechnol. 34 (2016) 394–407. http://10.1016/j.tibtech.2016.01.002.
[29] L.C. Czuba, K.M. Hillgren, P.W. Swaan, Post-translational modifications of transporters, Pharmacol. Ther. 192 (2018) 88–99. http://10.1016/j.pharmthera.2018.06.013.
[30] Y.R. Chen, X. Yan, F.Z. Yuan, Kartogenin-conjugated double-network hydrogel combined with stem cell transplantation and tracing for cartilage repair, Adv. Sci. 9 (2022). http://10.1002/advs.202105571.
[31] Y. Wang, G. Jones, C. Hill, Effect of atorvastatin on knee cartilage volume in patients with symptomatic knee osteoarthritis: results from a randomized placebo-controlled trial, Arthritis Rheumatol. 73 (2021) 2035–2043. http://10.1002/art.41760.
[32] L.S. Wang, J.E. Chung, P.P. Chan, M. Kurisawa, Injectable biodegradable hydrogels with tunable mechanical properties for the stimulation of neurogenesic differentiation of human mesenchymal stem cells in 3D culture, Biomaterials 31 (2010) 1148–1157. http://10.1016/j.biomaterials.2009.10.042.
[33] X. Li, J. Zhang, N. Kawazoe, G. Chen, Fabrication of highly crosslinked gelatin hydrogel and its influence on chondrocyte proliferation and phenotype, Polymers 9 (2017). http://10.3390/polym9080309.
[34] Y. Liu, S. Sakai, M. Taya, Impact of the composition of alginate and gelatin derivatives in bioconjugated hydrogels on the fabrication of cell sheets and spherical tissues with living cell sheaths, Acta Biomater. 9 (2013) 6616–6623. http://10.1016/j.actbio.2013.01.037.
[35] Y. Xu, Y. Xu, B. Bi, A moldable thermosensitive hydroxypropyl chitin hydrogel for 3D cartilage regeneration *in vitro* and *in vivo*, Acta Biomater. 108 (2020) 87–96. http://10.1016/j.actbio.2020.03.039.
[36] H. Liu, J. Liu, C. Qi, Thermosensitive injectable in-situ forming carboxymethyl chitin hydrogel for three-dimensional cell culture, Acta Biomater. 35 (2016) 228–237. http://10.1016/j.actbio.2016.02.028.
[37] Y. Liu, J. Lim, S.H. Teoh, Review: development of clinically relevant scaffolds for vascularised bone tissue engineering, Biotechnol. Adv. 31 (2013) 688–705. http://10.1016/j.biotechadv.2012.10.003.
[38] J. Cai, L.F. Liu, Z. Qin, Natural Morin-Based Metal Organic Framework Nanoenzymes Modulate Articular Cavity Microenvironment to Alleviate Osteoarthritis, 6, Wash D C), Research, 2023, p. 68. http://10.34133/research.0068.
[39] W. Ye, Z. Yang, F. Cao, H. Li, T. Zhao, H. Zhang, Z. Zhang, S. Yang, J. Zhu, Z. Liu, J. Zheng, H. Liu, G. Ma, Q. Guo, X. Wang, Articular cartilage reconstruction with TGF-β1-simulating self-assembling peptide hydrogel-based composite scaffold, Acta Biomater. 146 (2022) 94–106. http://10.1016/j.actbio.2022.05.012.
[40] W. Qian, R. Xin, W. Jian, Elastic fiber-reinforced silk fibroin scafflod with A double-crosslinking network for human ear-shaped cartilage regeneration, Advanced Fiber Materials 5 (2023) 1008–1024. https://10.1007/s42765-023-00266-8.
[41] K. Nie, S. Han, J. Yang, Enzyme-crosslinked electrospun fibrous gelatin hydrogel for potential soft tissue engineering, Polymers 12 (2020). http://10.3390/polym12091977.
[42] Y. Huo, Y. Xu, X. Wu, Functional trachea reconstruction using 3D-bioprinted native-like tissue architecture based on designable tissue-specific bioinks, Adv. Sci. 9 (2022). http://10.1002/advs.202202181.
[43] H. Wei, H. Huang, H. He, Pt-Se Hybrid Nanozymes with Potent Catalytic Activities to Scavenge ROS/RONS and Regulate Macrophage Polarization for Osteoarthritis Therapy, 7, Research (Wash D C), 2024, p. 310. http://10.34133/research.0310.
[44] J. Xu, Q. Feng, S. Lin, Injectable stem cell-laden supramolecular hydrogels enhance in situ osteochondral regeneration via the sustained co-delivery of hydrophilic and

hydrophobic chondrogenic molecules, Biomaterials 210 (2019) 51–61. http://10.1016/j.biomaterials.2019.04.031.

[45] D.C. Browe, P.J. Díaz-Payno, F.E. Freeman, R. Schipani, R. Burdis, D.P. Ahern, J. M. Nulty, S. Guler, L.D. Randall, C.T. Buckley, P.A.J. Brama, D.J. Kelly, Bilayered extracellular matrix derived scaffolds with anisotropic pore architecture guide tissue organization during osteochondral defect repair, Acta Biomater. 143 (2022) 266–281. http://10.1016/j.actbio.2022.03.009.

[46] B. Dai, Y. Zhu, X. Li, Z. Liang, S. Xu, S. Zhang, Z. Zhang, S. Bai, W. Tong, M. Cao, Y. Li, X. Zhu, W. Liu, Y. Zhang, L. Chang, P.S. Yung, H.K. Ki-Wai, J. Xu, T. Ngai, L. Qin, Blockage of osteopontin-integrin β3 signaling in infrapatellar fat pad attenuates osteoarthritis in mice, Adv. Sci. 10 (2023). http://10.1002/advs.202300897.

[47] M.P. Murphy, L.S. Koepke, M.T. Lopez, X. Tong, T.H. Ambrosi, G.S. Gulati, O. Marecic, Y. Wang, R.C. Ransom, M.Y. Hoover, H. Steininger, L. Zhao, M. P. Walkiewicz, N. Quarto, B. Levi, D.C. Wan, I.L. Weissman, S.B. Goodman, F. Yang, M.T. Longaker, C.K.F. Chan, Articular cartilage regeneration by activated skeletal stem cells, Nat. Med. 26 (2020) 1583–1592. http://10.1038/s41591-020-1013-2.